JOURNAL OF PROPULSION AND POWER
Vol. 21, No. 4, July–August 2005

Blade Forced Response Prediction for Industrial Gas Turbines

Stuart Moffatt*
University of Durham, Durham, England DH1 3LE, United Kingdom
Wei Ning,† Yansheng Li,‡ and Roger G. Wells§
ALSTOM Power U.K., Ltd., Lincoln, England LN5 7FD, United Kingdom
and
Li He¶
University of Durham, Durham, England DH1 3LE, United Kingdom

A decoupled aeromechanical system based on an advanced frequency-domain computational fluid dynamics finite element to CFD solver with fully nonlinear capability is presented that allows resonant vibration predictions to be routinely performed during the design process. A new energy method is presented that solves the blade response without the knowledge of original modeshape scales. A robust finite element CFD mesh interface has been developed for industrial use that can accurately deal with differences in mesh geometry, low mesh density, and high modeshape gradients. The capability of the baseline CFD solver for blade row interaction flow prediction is further validated against the von Kármán Institute transonic turbine stage. A forced response analysis is carried out on the NASA Rotor 67 transonic fan for demonstration purposes. The system is evaluated for a challenging industrial study of the ALSTOM three-stage transonic test compressor, where the forced response predictions of three crossing points on the Campbell diagram compare well with strain gauge test data. An investigation into aerodynamic damping of the first 10 modes shows a high dependency on modeshape.

Nomenclature

F	=	aerodynamic physical excitation force
f	=	aerodynamic modal excitation force
q	=	modal amplitude
W_d	=	aerodynamic damping work per vibratory cycle
W_f	=	aerodynamic forcing work per vibratory cycle
x	=	physical displacement amplitude
ζ	=	modal system damping ratio
ζ_{aero}	=	modal aerodynamic damping ratio
ϕ	=	mass-normalized mode shape
ω	=	natural frequency

Superscript

CFD	=	values for vibration amplitude of computational fluid dynamics damping calculation

Introduction

FLOW through gas-turbine engines is highly unsteady, where strong periodic flow disturbances can cause high amplitudes of blade vibration under certain resonant conditions. High-cycle fatigue failure due to excessive resonant stresses is a serious concern in both industrial gas-turbine and aeroengine applications where it has been known to cause catastrophic engine failure. The need to predict dangerous resonant conditions in the design stage is becoming more apparent with modern engine designs, where increased blade loading and reduced axial spacing challenge the capabilities of conventional empirical design rules. The ability to assess potential vibration problems before manufacture can provide significant benefits in terms of reduced development costs and lead times and improved reliability.

Received 29 October 2003; revision received 25 October 2004; accepted for publication 19 October 2004.

*Research Associate, School of Engineering.
†Principal Engineer, P.O. Box 1, Compressor Group, Waterside South.
‡Compressor Specialist, P.O. Box 1, Compressor Group, Waterside South.
§Technology Manager, P.O. Box 1, Compressor Group, Waterside South.
¶Professor of Thermo-Fluids Engineering, School of Engineering.

A common design practice is to calculate the blade natural frequencies and plot the Campbell diagram, mapping the natural frequencies to the engine speed and excitation orders. The blades are designed with the intention of avoiding resonance by placing natural frequencies outside the normal operating speeds, where they will not be encountered during normal operation. However, modes placed below the normal operating speed cannot be avoided and are excited during every operational cycle at startup and shutdown, contributing to blade fatigue. Resonant stresses at these points are often estimated using empirical rules based on past experience. Structural integrity is verified by engine testing, at which stage the discovery of vibration problems can incur great cost. However, routine forced vibration predictions at the design stage are generally limited to the larger aeroengine manufacturers due to the high computational demands of three-dimensional unsteady flow solvers. The need for fully three-dimensional calculations around vibrating blades has great implications on computing time and has often been reported, such as by Bell and He.[1]

Fluid–structure coupling poses difficult modeling issues for forced response prediction due to the interaction between the blade motion and the unsteady flowfield. Incoming periodic flow disturbances provide excitation of the blade, causing forced vibration. Consequently, the motion of the blade induces an unsteady pressure field around the blade, resulting in aerodynamic damping for forced response cases (negative damping for flutter). Various fully coupled and decoupled forced response prediction methods have been developed.

Fully coupled time-marching schemes have combined sophisticated three-dimensional viscous/inviscid multistage models with various structural dynamics methods.[2,3] Computational demands are often too high for routine use due to the requirement for high temporal resolution and multipassage or whole-annulus domains.

The linearized decoupled method provides a highly efficient frequency-domain approach, assuming linear aerodynamic damping and assuming that mode shapes and natural frequencies are not affected by aerodynamic loading. These assumptions are generally valid for turbomachinery blades that are of high density and stiffness and that vibrate at low amplitudes. Linear aerodynamic damping behavior for two transonic fan rotors has been observed by Li and He[4] and Schmitt et al.[5] For forced response applications, linear flow solvers combined with the decoupled method have been reported for both resonant[6–8] and transient forced vibration problems.[9] The use

of nonlinear time-marching schemes with the decoupled method, although less common, has been reported by Schmitt et al.[5] and Moyroud et al.[10]

The advantage of the decoupled method is recognized in this paper by employing the efficient frequency-domain nonlinear harmonic flow solver of He et al.[11] that is 30–100 times faster than equivalent time-marching schemes. Fully nonlinear flow can be included by closely coupling the solution of the unsteady perturbation equations with those of the time-averaged flow, with the option of cross coupling the individual flow harmonics.[12] Validation of the baseline solver against semi-analytical solutions is given by Vasanthakumar et al.[13] for vibrating inviscid flow through unloaded two-dimensional and three-dimensional flat-plate cascades and by Chen et al.[14] for wake–blade interaction in a uniform steady flow past an unloaded flat-blade cascade. Chen et al. also verify the nonlinear capability of the nonlinear harmonic method for a single-stage compressor by comparing the deterministic stresses with those obtained from nonlinear time marching in both two and three dimensions. Verification on the use of the linear method for blade row interaction in a subsonic turbine stage and a transonic counter-rotating prop fan is provided by Ning et al.,[15] who show qualitative and quantitative agreement with test data and nonlinear time-accurate solutions. The ability of the linearized method to predict blade row interaction is further verified in this paper against test data for a transonic turbine stage.

In the presented aeromechanical system, resonant blade vibration is modeled linearly based on modal decoupling using two distinct approaches: 1) solution of the modal equation and 2) a new energy method. Modal reduction solves a single-degree-of-freedom (SDOF) dynamic equation in modal space using well-established theory and involves the transformation of physical properties into modal space. The energy method requires no knowledge of modeshape scales, directly solving the blade vibration on the computational fluid dynamics (CFD) mesh by means of an energy balance. The methodologies are demonstrated in this paper with an analysis of the forced vibration of the NASA Rotor 67 transonic fan rotor caused by a hypothetical inlet distortion to emulate a practical problem. The system is finally used to model the forced vibration of the last stage rotor of the ALSTOM three-stage transonic test compressor. Predicted resonant strain levels for three high-order modes are compared with strain-gauge measurements, and the variation of aerodynamic and mechanical damping with modeshape are investigated. Further details of the cases and methodologies presented herein are provided by Moffatt and He[16] and Ning et al.[17]

Forced Response Prediction System

Shown in Fig. 1, the methodology of the forced response prediction system represents an open-loop approach, requiring a single execution of the fluid and structural calculations. Mode shapes and natural frequencies are obtained from a finite element (FE) modal analysis, from which a single mode is selected using the Campbell diagram and then interpolated onto the CFD mesh. With aerodynamic boundary conditions obtained from the performance map, the aerodynamic forcing and damping calculations are performed separately, yielding the harmonic pressures at the blade natural frequency. The three-dimensional Navier–Stokes (N–S) equations are solved in the frequency domain using a single-passage approach. Aerodynamic forcing is obtained from a multistage CFD calculation through passages with rigid blades. The aerodynamic damping calculation is performed on an isolated blade row with clean incoming flow and the blades vibrating in the specified mode to yield the aerodynamic damping work. The vibration amplitude is fixed at a realistic level, and the interblade is determined by the wavelength of the excitation forces.

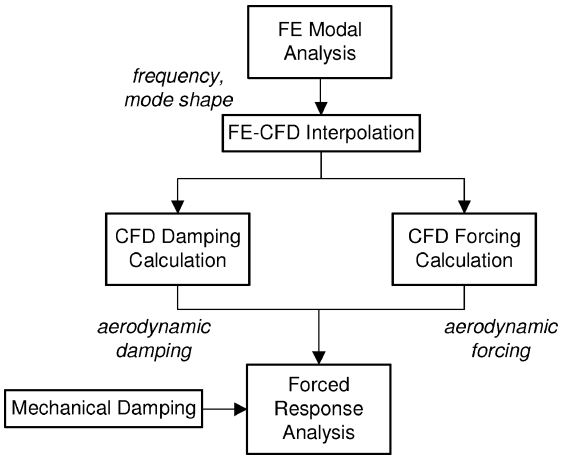

Fig. 1 Forced response prediction methodology.

Resonant forced vibration is modeled on the CFD mesh with great efficiency, scaling the mode shape with an SDOF equation using two distinct approaches. The modal method is based on well-established modal reduction theory and involves a transformation of physical properties into modal space before analytically solving the modal equation. The solution is directly applied to either the CFD or FE mesh to yield physical displacement, stress, or strain amplitudes. The energy method provides an alternative to the modal approach that eliminates the need for mass-normalized modeshapes. The blade motion is scaled to balance stabilizing (damping) and destabilizing (forcing) work to provide the blade response at equilibrium.

The decoupled approach is not limited to linear flow conditions, where the nonlinear harmonic solver can include nonlinearities with great efficiency. Nonlinear forcing terms are independent of blade motion and are included intrinsically in the decoupled method. For cases where damping is suspected to be nonlinear, the damping calculation can simply be restarted at the solution amplitude without a large increase in total computing time, before repeating the solution of the modal equation.

Flutter calculations can be carried out using only the damping part of the decoupled approach, neglecting the forcing effects of inlet distortion and blade row interaction. The stability of a mode under particular flow conditions and interblade phase angle is given simply by the aerodynamic damping work. A positive value of work applied to the blade by the fluid indicates instability (negative aerodynamic damping). Although this method of flutter prediction is well-established, a recent extension of the approach by Chen et al.[18] uses an energy method to find vibration levels where the flutter limit can be found.

Methodologies

FE–CFD Interpolation

The FE–CFD interface must be robust enough to interpolate the modeshape from any unstructured FE mesh onto the CFD mesh accurately, while coping with high modeshape gradients, low mesh densities, and node indexing issues. Further complications arise due to differences in mesh geometry, where the FE mesh geometry is usually modified to allow for the effects of centrifugal, gas, and temperature loading. This geometry mismatch usually causes the boundary surfaces of the two meshes to be noncoincident. A method of interpolation is presented that can accurately translate a modeshape on an unstructured FE mesh consisting of any combination of tetrahedral, hexahedral, prismatic, and wedge elements to the solid boundary of a CFD mesh, while overcoming the aforementioned difficulties.

The modeshape amplitudes are transferred by two-dimensional linear interpolation over the three-dimensional mesh surface, based on the mean position of the blade. For each CFD surface point on the solid boundary, an interpolation plane is selected on the FE mesh surface defined by the positions of three FE nodes. The three nodes, belonging to the external face of a finite element, form a triangle, and the nodes are selected to give the closest centroid to the CFD node. For any rectangular face, the four possible interpolation planes are shown in Fig. 2. If the CFD point does not coincide with the plane, two-dimensional linear interpolation is taken at the point of orthogonal projection of the CFD point onto the plane, as shown in Fig. 3. This approach is thought to be more accurate than three-dimensional interpolation using the FE shape functions because only the surface modeshape values are of interest.

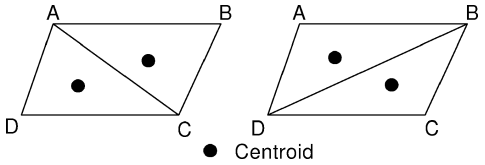

Fig. 2 Possible interpolation planes on a rectangular FE face.

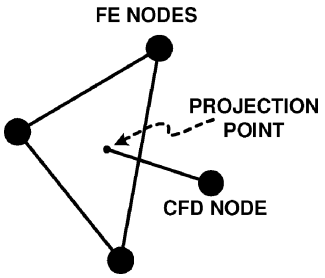

Fig. 3 Two-dimensional interpolation at projection on FE mesh surface.

To improve accuracy with low-density FE meshes, averaging is performed over adjacent structural elements at regions close to element edges. External faces of the FE mesh that are aligned normal to the suction and pressure surfaces, such as the leading, trailing, and tip edges, can cause errors when used for interpolation. Whereas the errors may be minimal for high-density FE meshes, low-density meshes may require the identification of such faces. CFD meshes containing tip clearance cells are dealt with by linearly reducing radial motion at the tip to zero at the casing and setting axial and tangential modeshape components equal to the tip. The accuracy of the interpolation for an industrial case is demonstrated later in the ALSTOM compressor case study.

Forced Response Solution

The resonant vibration of the lightly damped structure allows an SDOF equation to model the blade motion by scaling the modeshape by the modal amplitude. Modeshapes from the FE modal analysis are scaled to unity modal mass, allowing the modal equation to be represented as

$$\ddot{q} + 2\zeta\omega\dot{q} + \omega^2 q = f \tag{1}$$

where f is the aerodynamic modal force and ζ is the modal system damping ratio. The complex modal force is obtained by taking the dot product of the mass-normalized modeshape vector and the complex aerodynamic force vector using

$$\tilde{f} = \sum_{k=1}^{n} \left\{ \phi_k \cdot (F^{\text{Real}} + \boldsymbol{i} F^{\text{Imag}})_k \right\} \tag{2}$$

where F^{Real} and F^{Imag} are the complex components of the aerodynamic force amplitude acting on each DOF k and n is the number of DOF in the FE model. The aerodynamic damping ratio ζ_{aero} is calculated using the principle of equivalent viscous damping by

$$\zeta_{\text{aero}} = \frac{-W_d^{\text{cfd}}}{2\pi\omega^2 (q^{\text{cfd}})^2} \tag{3}$$

where W_d^{cfd} is the damping work at the modal amplitude of the CFD damping calculation q^{cfd}. Equation (1) is solved analytically to yield the modal amplitude. Physical solution amplitudes are obtained by directly scaling normalized modeshapes, stress, or strain distributions by the modal amplitude on either the FE or CFD mesh.

Energy Method

The energy method is a simple approach to solving the forced response problem by means of an energy balance, eliminating the use of modal reduction theory. Modeshapes can be scaled freely, disregarding the original normalized scales and units. Steady-state vibration occurs when the forcing (destabilizing) work applied to the blade balances the dissipated damping (stabilizing) work. Based on a linear increase of forcing work with vibration amplitude and a quadratic increase of damping work, a single point of equilibrium can be found, yielding the solution amplitude as shown in Fig. 4.

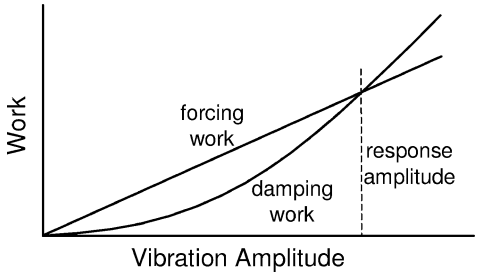

Fig. 4 Equilibrium of forcing and damping work.

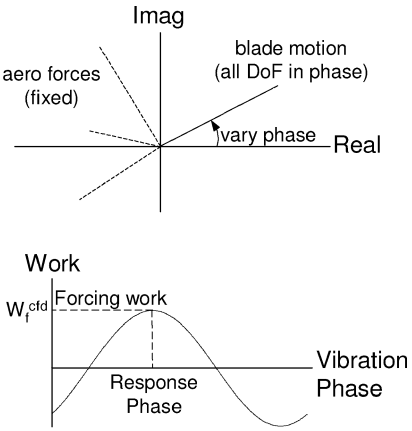

Fig. 5 Response phase for maximum forcing work.

Aerodynamic forcing and damping work are calculated at the vibration amplitude used for the CFD damping calculation. Forcing work is obtained when the following are known: 1) Aerodynamic forces are not affected by blade motion. 2) The vibration will lag the force distribution with the phase, providing the maximum destabilizing effect. In other words, the modeshape lags the forcing by the angle providing the maximum work to the blade. For harmonic motion and forcing, the forcing work follows a sinusoidal variation with vibration phase. A simple iterative approach calculates the work done on the blade at discrete angles varying between 0 and 2π to obtain the maximum work, as shown in Fig. 5. The forcing and damping work is then scaled to find the point of equilibrium, given by

$$\{x^{\text{FR}}\} = \left(-W_f^{\text{cfd}} \big/ W_d^{\text{cfd}}\right)\{x^{\text{cfd}}\} \tag{4}$$

where the original blade motion $\{x^{\text{cfd}}\}$ used in the damping calculation is scaled to provide the blade response $\{x^{\text{FR}}\}$.

Case Studies

Von Kármán Institute for Fluid Dynamics (VKI) BRITE-EuRAM Transonic Turbine Stage

The von Kármán Institute for Fluid Dynamics (VKI) BRITE-EuRAM transonic turbine has previously been used in a large test program, as published by Dénos et al.[19] and Valenti et al.[20] Consisting of 43 vanes and 64 blades, 24 pressure transducers were located on the rotor blade surface at each span position of 15, 50, and 85%. In this paper, the unsteady flow is calculated using the time-linearized N–S solver at the normal operating condition with a total pressure ratio of 2.69 and a Reynolds number of 10^6. A simple H mesh was used, consisting of almost 0.5 million mesh points for the vane and blade passage using a single-passage approach. The 3% coolant flow ejected from the vane trailing edge is neglected in the present calculation; instead a rounded trailing edge is used. The three-dimensional nonlinear calculation by Laumert et al.[21] indicated an insignificant effect of the trailing-edge cut on the steady flow.

Providing a basis for the time-linearized unsteady calculation, the steady flow through the turbine is calculated utilizing the mixing

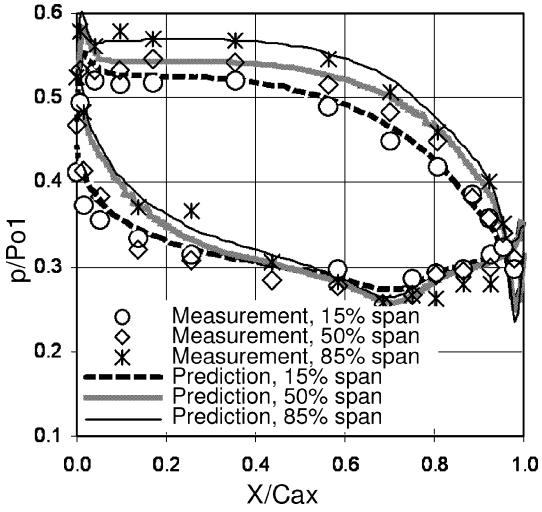

Fig. 6 Rotor blade surface pressure distributions.

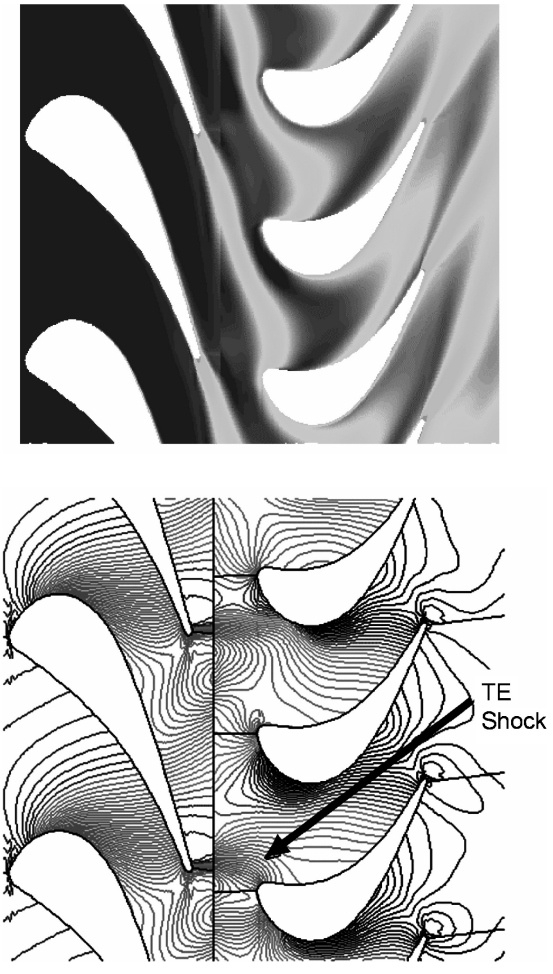

Fig. 7 Instantaneous entropy contours at midspan.

plane at the vane–rotor interface. A comparison between the predicted surface pressures on the blade with the test data at three spanwise locations is shown in Fig. 6. Whereas good agreement is observed for the 15 and 85% sections, it is not apparent why the flow acceleration at the front of the suction surface at 50% span is underpredicted. The numerical predictions of Dénos et al.[19] and Laumert et al.[21] show similar underpredictions around this region.

The linear calculation is performed in a single vane and rotor blade passage, preserving the true blade count. The vane wake and potential waves are resolved by the first three harmonics. With the instantaneous entropy contours at 50% span as shown in Fig. 7, the downstream convection of vane wakes and interaction of the vane trailing-edge shock can be seen to be well-captured. A comparison of the predicted and measured pressures acting on the blade is provided in Fig. 8 in the form of amplitude and phase. A high unsteady pressure amplitude around the blade leading region can be seen to be caused by the vane trailing-edge shock sweeping past that area. The linear solver predicts the unsteady pressure with fairly good accuracy, with the pressure increase from midspan to hub being captured particularly well.

Forced Response of NASA Rotor 67 Transonic Fan

The NASA Rotor 67 transonic fan rotor is presented to demonstrate the methodology of the decoupled system. The rotor consists of 22 low-aspect-ratio blades and is designed to produce a total pressure ratio of 1.63 for a mass flow rate of 32.25 kg/s with a tip inlet relative Mach number of 1.38 at the design point of speed 16,043 rpm. The baseline steady solver has been validated for this case against experimental data by Li and He.[4]

The FE model (Fig. 9) was simplified to a cantilevered aerofoil due to the lack of root geometry. It consists of 806 quadratic brick elements with a blade thickness of one element and uses typical material properties for titanium. With account taken of centrifugal loading, the first five natural frequencies from the modal analysis are given in Table 1.

By the use of a CFD H-mesh of $110 \times 25 \times 29$, the blade count was reduced to 21 to compare results with previous work. Because a single-passage domain was used, no computational benefit was gained from this. The blade is excited by a hypothetical seven-node inlet distortion at a blade passing frequency equal to the first torsion natural frequency at a rotor speed of 102.2%. The seven-node pattern was chosen to provide excitation of the mode close to normal operating speed.

The targeted sinusoidal distortion of 15% axial velocity at inlet was smeared around the casing (Fig. 10). This is likely to be caused by upstream-traveling pressure disturbances and viscous effects due to the low mesh density at the solid boundary. The pressure distribution over the blade resulting in a modal force of $f = (-19.1 + \boldsymbol{i}37.0)$ N and an aerodynamic forcing work of $W_f^{\text{cfd}} = 0.00634$ J/cycle. For the damping calculation, the mode-shape was scaled to give a leading-edge (LE) amplitude of 0.93 mm (1% chord) with a modal amplitude of $q^{\text{cfd}} = 4.86e-5$, yielding a damping work of $W_d^{\text{cfd}} = -0.0119$ J/cycle and a damping ratio of 0.56%. When the mechanical damping is neglected, the solution of the modal equation gives a modal amplitude of $2.58e-5$, corresponding to a tip LE amplitude of 0.49 mm and a maximum alternating stress of 74 MPa. The energy method gives an identical solution, as shown in Table 2, where the original blade motion used in the damping calculation is scaled by a factor of 0.531 to give the solution response.

Table 1 First five natural frequencies for NASA Rotor 67

Mode no.	Frequency
1	601.0
2	1307.9
3	1913.2
4	2740.6
5	3148.2

Table 2 Energy method forced vibration solution

Parameter	Value
W_f^{CFD}, J/cycle	0.00634
W_d^{CFD}, J/cycle	−0.0119
$W_f^{\text{CFD}} / W_d^{\text{CFD}}$	0.531
Tip LE amplitude, mm	0.49

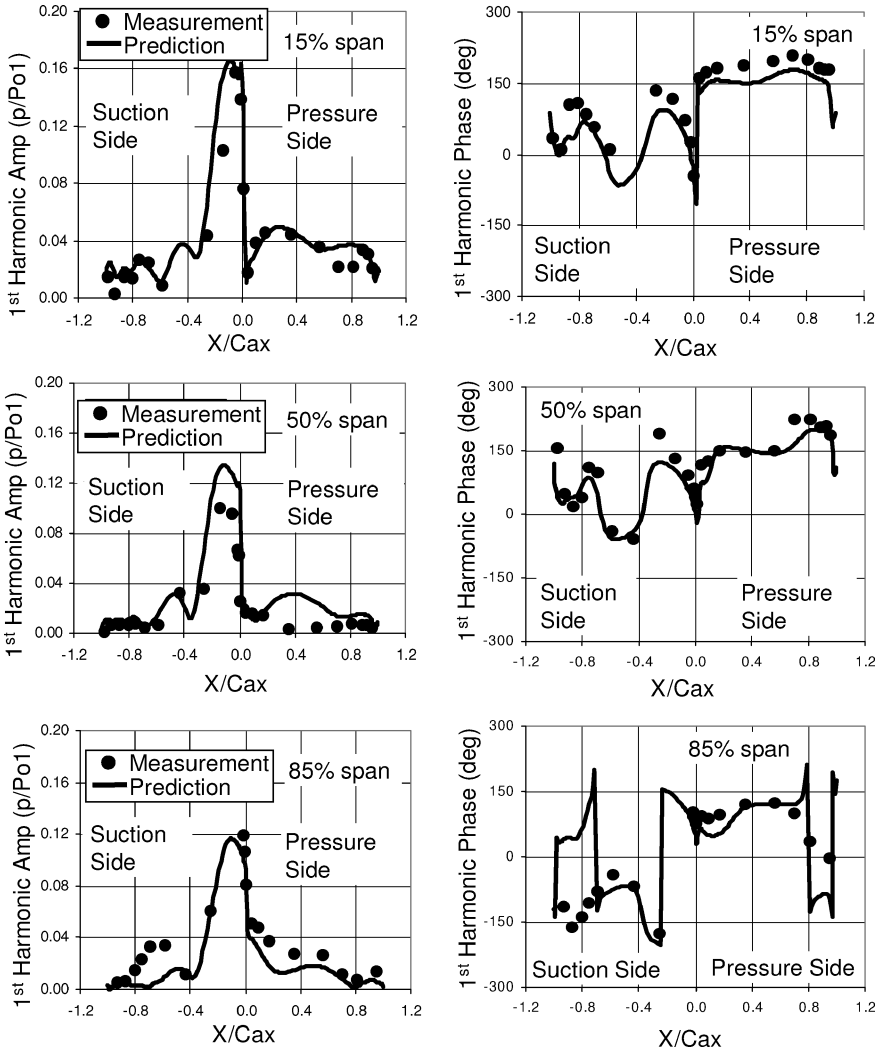

Fig. 8 Rotor blade surface unsteady pressure at vane passing frequency.

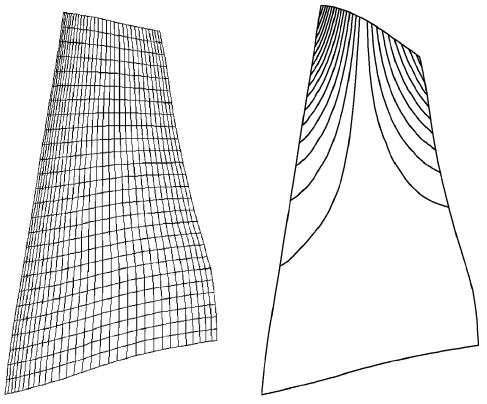

Fig. 9 FE mesh and first torsion mode.

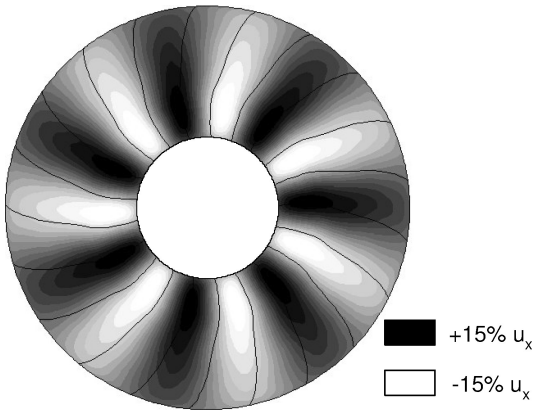

Fig. 10 Inlet axial velocity distortion.

ALSTOM Three-Stage Transonic Test Compressor

The ALSTOM three-stage test compressor (Fig. 11) is designed to operate at a mass flow rate of 26.3 kg/s at a pressure ratio of 3:1 (Li and Wells[22]). The compressor, which consists of an inlet guide vane, stage 0, 1, and 2, has previously been tested to evaluate aerodynamic performance and structural integrity. Speed sweeps were carried out to map vibration characteristics with strain gauges applied to three blades in each row. In this paper, the vibration of the last rotor induced by the adjacent upstream stator wake is calculated and compared with strain gauge measurements averaged over the three instrumented blades in the row.

The steady flow calculations are compared with measurements at 90 and 100% design speed in Fig. 12. Modeling each blade passage with 200,000 mesh points, giving a total of 1.5 million, gives good agreement between prediction and measurements. However, efficiency is underpredicted by 1% at 90% speed.

An FE analysis of the blade was carried out using a mesh comprising 1136, 20-node brick elements to provide modeshapes and the natural frequencies forming the Campbell diagram in Fig. 13. Modes 8, 9, and 10, shown in Fig. 14, are selected for analysis, crossing the 32 engine ordar (EO) interface at 84, 90, and 104% speed. Good

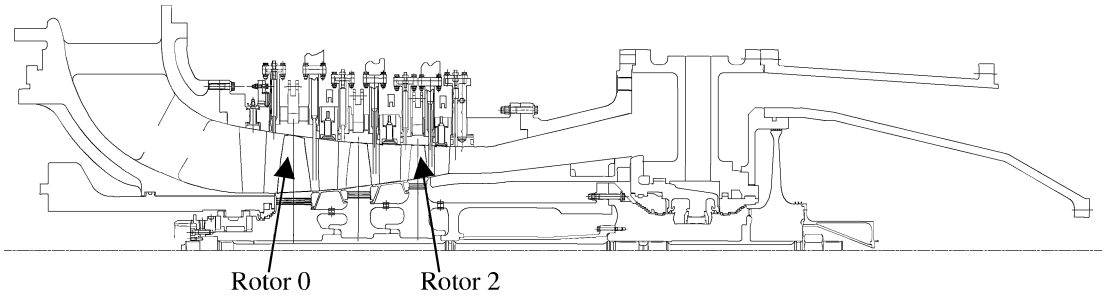

Fig. 11 Cross section of the ALSTOM three-stage transonic compressor.

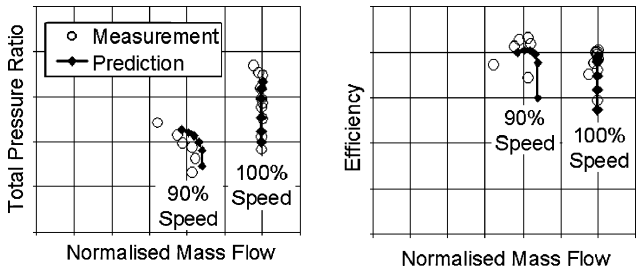

Fig. 12 ALSTOM three-stage compressor performance map.

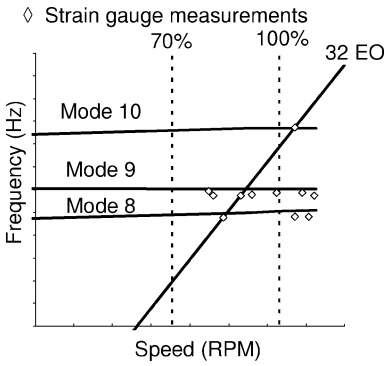

Fig. 13 Campbell diagram of rotor 2.

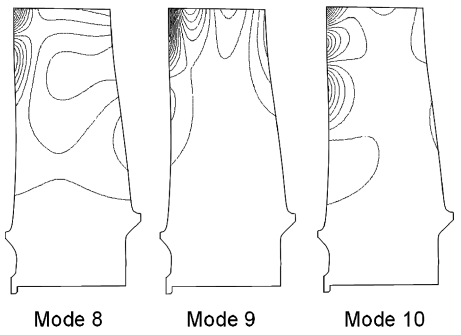

Fig. 14 Rotor 2 modeshapes.

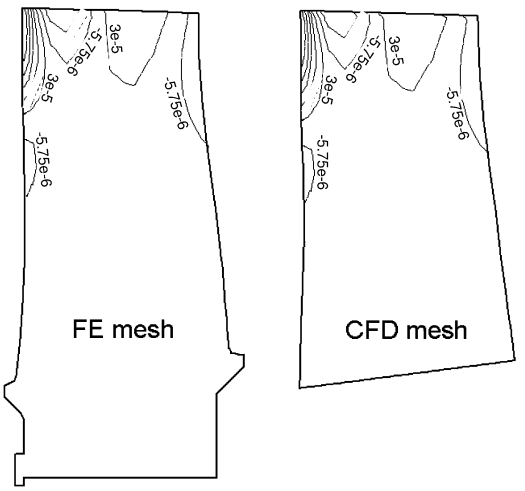

Fig. 15 Comparison of original and interpolated modeshape data for mode 9 of rotor 2.

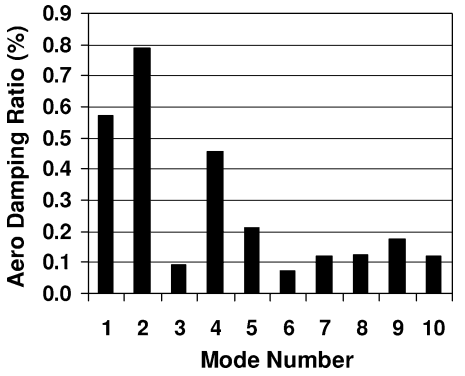

Fig. 16 Aerodynamic damping ratios.

Table 3 Aerodynamic and mechanical damping ratios

Damping ratio	Mode 8/32 EO, %	Mode 9/32 EO, %	Mode 10/32 EO, %
ζ_{aero}	0.11	0.17	0.13
ζ_{mech}	0.24	Negligible	Negligible

agreement between the predicted and measured frequencies can be seen. Originally positioned to capture the low-order modes, the strain gauges are located near the hub trailing edge, providing a reasonable strain gauge sensitivity factor of 15% for mode 8, but lower factors for modes 9 and 10. Figure 15 shows very high accuracy in the interpolation of mode 9 onto the CFD mesh, while demonstrating the ability to overcome difficulties due to high modeshape gradients, low mesh density, geometry mismatch, and tip clearance cells.

To find out the dependence of damping on modeshape, linear solutions were carried out on the first 10 modes at 90% speed with fixed inter-blade phase angle based on the stator 2 and rotor 2 blade counts. As seen in Fig. 16, damping has a large dependency on modeshape with higher damping generally observed for low-order modes but with modes 3 and 6 showing exceptionally low values. The predictions of the first four modes agree reasonably well with those quoted by Kielb and Imregun.[23] To compare aerodynamic with mechanical damping, system damping was calculated using the half-power rule on the strain gauge frequency response, then mechanical damping was taken as the difference between system and aerodynamic damping. The comparison in Table 3 shows significant mechanical damping for mode 8 and negligible damping for modes 9 and 10. Primarily due to friction at the blade root/disk interface, the minimal displacement at root for modes 9 and 10 explains

Table 4 Comparisons of predicted and measured strain

Crossings	Error of prediction from measurement, %
Mode 8/32EO	8
Mode 9/32EO	65
Mode 10/32EO	4

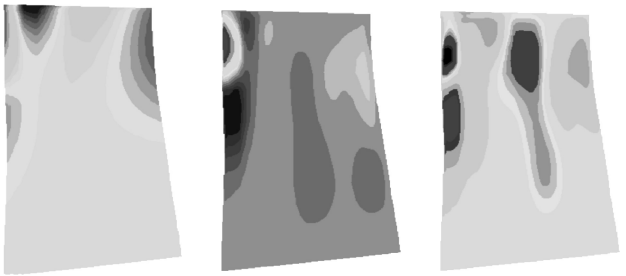

a) Axial displacement **b) Real modal force component** **c) Imaginary modal force component**

Fig. 17 Rotor 2 axial modeshape and axial modal force contributions for mode 9/32EO crossing.

the negligible damping. Whereas forced vibration prediction is dependent on system damping, many efforts have recently been made on aerodynamic damping prediction, but the predictive capability for mechanical damping is immature.

The unsteady flow from the upstream stator is calculated using the multistage time-linearized N–S solver at each of the blade passing frequencies (32EO), basing the rotor 2 inlet conditions on the multistage steady solution. Figure 17 shows the contribution of complex axial forces to the modal force. This shows the regions providing high structural excitation where high-pressure amplitudes coincide with large modeshape amplitudes (such as at the upper leading and trailing edges).

The resulting modal force is used together with the predicted aerodynamic damping and mechanical damping to calculate the resonant displacements and strains for each mode. The forced response calculation was repeated with the energy method to give identical results; therefore, the energy method is a useful tool for checking the modal solution. Table 4 shows the level of agreement between the predicted and measured strain. The mode 8 and 10 predictions show very good agreement. The higher error of mode 9 is believed to be due to the strain gauge being positioned in a high modeshape gradient for that mode, where the strain measurement is highly sensitive to position.

For each mode analyzed, the turnaround time is only a few hours on a typical workstation, largely due to the use of a linearized N–S solver. As discussed earlier, the methodology presented is not restricted to linear flow conditions. The low computing requirements and ease of implementation of the methodologies presented allows forced response prediction to become a routine part of the design process.

Conclusions

The methodology of a decoupled aeromechanical analysis system has been presented for the prediction of resonant forced vibration levels and flutter stability. Flow is modeled using a multistage frequency-domain unsteady CFD code, capable of dealing with flow nonlinearities. Blade vibration is modeled very efficiently using an SDOF equation based on modal decoupling. An alternative energy method is presented that solves the blade response directly on the fluid mesh and requires no knowledge of modeshape scales. An FE–CFD mesh interface that is robust enough to deal with the complexities of industrial use is discussed and validated.

The capability of the CFD solver to predict unsteady flow due to blade row interaction has been demonstrated against the VKI transonic turbine stage. The ease of implementation of the decoupled method has been demonstrated with a case study of the NASA Rotor 67 transonic fan, where vibration levels due to a hypothetical inlet distortion are calculated.

The system was applied to model the vibration of the last stage rotor of the ALSTOM three-stage transonic test compressor caused by interference from the upstream stator wakes at three crossing points on the Campbell diagram. The damping calculations have shown that aerodynamic damping is strongly influenced by modeshape, and a comparison with strain-gauge data also indicates a strong correlation between mechanical damping and modeshape. Predicted resonant strains for the three crossing points were compared with strain-gauge measurement with reasonably good agreement, demonstrating the ability of the method to predict resonant vibration levels. The high efficiency of the unsteady multistage calculation also demonstrates that the system can be used routinely in the blade design process to tackle aeromechanical issues. The modal and energy methods produced identical results for both forced response cases.

Acknowledgments

This research is funded by the European Union Framework V research and development project "Development of Innovative Techniques for Compressor Aero-Mechanical Design (DITCAD)," Contract ENK5-CT-2000-00086. The nonlinear harmonic method has been developed by L. He, W. Ning, T. Chen, and P. Vasanthakumar, University of Durham, under sponsorship from ALSTOM Power U.K., Ltd. The von Kármán Institute for Fluid Dynamics (VKI) turbine stage was carried out under contract for the European Commission as part of the BRITE EuRAM III BE97-4440 project "Turbine Aero-Thermal External Flows." The authors would like to thank R. Dénos of VKI for the useful discussions on the VKI turbine-stage case and the management of ALSTOM Power U.K., Ltd. for permission to publish this paper.

References

[1]Bell, D. L., and He, L., "Three-Dimensional Unsteady Flow for an Oscillating Turbine Blade and the Influence of Tip Leakage," *ASME Journal of Turbomachinery*, Vol. 122, No. 1, Jan. 2000, pp. 93–101; also American Society of Mechanical Engineers, Paper ASME 98-GT-571, 1998.

[2]Bréard, C., Vahdati, M., Sayama, A. I., and Imregun, M., "An Integrated Time-Domain Aeroelasticity Model for the Prediction of Fan Forced Response due to Inlet Distortion," American Society of Mechanical Engineers, Paper ASME 2000-GT-0373, 8–11 May 2000.

[3]Vahdati, M., Sayama, A., and Imregum, M., "Case Studies in Turbomachinery Aeroelasticity Using an Integrated 3D Non-linear Method," VKI Lecture Series, 1999–05, von Kármán Inst. for Fluid Dynamics, Rhode-Saint-Genèse, Belgium, 1999.

[4]Li, H. D., and He, L., "Single-Passage Analysis of Unsteady Flows Around Vibrating Blades of a Transonic Fan Under Inlet Distortion," *ASME Journal of Turbomachinery*, Vol. 124, No. 2, April 2002, pp. 285–292; also American Society of Mechanical Engineers, Paper ASME 2001-GT-272, 2001.

[5]Schmitt, S., Nürnberger, D., and Carstens, V., "Evaluation of the Principle of Aerodynamic Superposition in Forced Response Calculations," *10th International Symposium on Unsteady Aerodynamics, Aeroacoustics and Aeroelasticity in Turbomachines*, Duke Univ., Durham, NC, 2003.

[6]Kielb, R. E., "Forced Response Design Analysis," *Aeroelasticity in Axial-Flow Turbomachines*, VKI Lecture Series 1999–05, von Kármán Inst. for Fluid Dynamics, Rhode-Saint-Genèse, Belgium, 1999.

[7]Chiang, H. D., and Kielb, R. E., "An Analysis System for Blade Forced Response," *Journal of Turbomachinery*, Vol. 115, pp. 762–770.

[8]Manwaring, S. R., and Kirkeng, K. L., "Forced Response Vibrations of a Low Pressure Turbine Due to Circumferential Temperature Distortions," *8th International Symposium on Unsteady Aerodynamics, Aeroacoustics and Aeroelasticity in Turbomachines*, edited by T. H. Fransson, Kluwer Academic, The Netherlands, 1997.

[9]Green, J. S., and Marshall, J. G., "Forced Response Prediction within the Design Process," *3rd European Conference on Turbomachinery*, IMEHE Paper C557/121/99, March 1999.

[10]Moyroud, N., Cosme, N., Jöker, M., Fransson, T. H., Lornage, D., and Jacquet-Richardet, G., "A Fluid-Structure Interfacing Technique for Computational Aeroelastic Simulations," *The 9th International Symposium on Unsteady Aerodynamics, Aeroacoustics and Aeroelasticity in Turbomachines*, edited by P. Ferrand and S. Aubert, Presses Universitaires de Grenoble, Grenoble, France, 2000.

[11]He, L., Chen, T., Wells, R. G., Li, Y. S., and Ning, W., "Analysis of Rotor–Rotor and Stator–Stator Interferences in Multi-Stage Turbomachines," *Journal of Turbomachinery*, Vol. 124, No. 4, 2002, pp. 564–571.

[12]Vasanthakumar, P., "Three Dimensional Frequency-Domain Solution Method for Unsteady Turbomachinery Flows," Ph.D. Dissertation, School of Engineering, Univ. of Durham, Durham, England, U.K., 2003.

[13]Vasanthakumar, P., Chen, T., and He, L., "Three-Dimensional Viscous Computation of Blade Flutter and Forced Response Using Nonlinear Harmonic Approach," *9th International Symposium on Unsteady Aerodynamics, Aeroacoustics and Aeroelasticity in Turbomachines*, edited by P. Ferrand and S. Aubert, 2000, Presses Universitaires de Grenoble.

[14]Chen, T., Vasanthakumar, P., and He, L., "Analysis of Unsteady Bladerow Interaction Using Nonlinear Harmonic Approach," *Journal of Propulsion and Power*, Vol. 17, No. 3, 2001, pp. 651–658.

[15]Ning, W., Li, Y. S., and Wells, R. G., "Predicting Bladerow Interactions Using a Multistage Time-Linearized Navier–Stokes Solver," *Journal of Turbomachinery*, Vol. 125, No. 1, 2003, pp. 25–31; also American Society of Mechanical Engineers, Paper ASME 2002-GT-30309, June 2002.

[16]Moffatt, S., and He, L., "Blade Forced Response Prediction for Industrial Gas Turbines, Part 1: Methodologies," American Society of Mechanical Engineers, Paper ASME GT2003-38642, 16–19 June 2003.

[17]Ning, W., Moffatt, S., Li, Y., and Wells, R. G., "Blade Forced Response Prediction for Industrial Gas Turbines, Part 2: Verification and Application," American Society of Mechanical Engineers, Paper ASME GT2003-38642, 16–19 June 2003.

[18]Chen, Z., Hong, L., and Xiaofeng, W., "Full-Function Numerical Method for Flow Over a Self-Excited Vibrating Body," *Tsinghua Science and Technology*, Vol. 4, No. 4, 1999.

[19]Dénos, R., Siverding, C. H., Arts, T., Brouckaert, J. F., Paniagua, G., and Michelassi, V., "Experimental Investigation of Unsteady Rotor Aerodynamics of a Transonic Turbine Stage," *Institution of Mechanical Engineers Conference Transactions*, pp. 271–287; also *Journal of Power and Energy*, Vol. 23, No. A4, 1999, pp. 327–338.

[20]Valenti, E., Dénos, R., Art, T., and Halama, J., "Investigation of the 3D Unsteady Rotor Pressure Field in a HP Turbine Stage," American Society of Mechanical Engineers, Paper ASME GT-2002-30365, 2002.

[21]Laumert, B., Martensson, H., and Fransson, T. H., "Investigation of the Flowfield in the Transonic VKI BRITE EURAM Turbines Stage with 3D Steady and Unsteady N–S Computations," American Society of Mechanical Engineers, Paper ASME 2000-GT-433, 2000.

[22]Li, Y. S., and Wells, R. G., "The Three-Dimensional Aerodynamic Design and Test of a Three-Stage Transonic Compressor," American Society of Mechanical Engineers, Paper ASME 99-GT-068, 1999.

[23]Kielb, R. E., and Imregun, M., "Aeroelasticity in Axial Flow Turbomachines—Damping Characteristics," *Aeroelasticity in Axial-Flow Turbomachines*, VKI Lecture Series 1999–05, von Kármán Inst. for Fluid Dynamics, Rhode-Saint-Genèse, Belgium, 1999.